THE JOURNAL OF PHYSICAL CHEMISTRY C
A JOURNAL OF THE AMERICAN CHEMICAL SOCIETY

pubs.acs.org/JPCC

Article

Exciton Photoluminescence of Strongly Quantum-Confined Formamidinium Lead Bromide ($FAPbBr_3$) Quantum Dots

Published as part of The Journal of Physical Chemistry virtual special issue "Horst Weller Festschrift".

Xueting Tang, Mohit Khurana, Daniel Rossi, Lanyin Luo, Alexey V. Akimov, and Dong Hee Son*

Cite This: *J. Phys. Chem. C* 2022, 126, 18366−18373

Read Online

ACCESS | Metrics & More | Article Recommendations | Supporting Information

ABSTRACT: Imposing strong quantum confinement in metal halide perovskite (MHP) quantum dots (QDs) not only tunes the exciton transition energy but also alters other photophysical properties that are sensitive to the spatial confinement of the exciton wave function. A recent study of inorganic cesium lead halide QDs in strongly confined regime revealed important exciton properties contrasting to those of weakly confined counterparts, such as the strong emission from the dark exciton and switching of the relative level order of bright and dark states. However, strongly quantum-confined hybrid MHP QDs, with organic A-site cations that are known to have additional pathways to influence the exciton and charge carrier transport properties in bulk, have received less attention. Here, we prepared strongly quantum-confined formamidinium lead bromide ($FAPbBr_3$) QDs of different sizes and studied the photoluminescence, fine structure, and decay dynamics of excitons at varying temperatures and under varying magnetic fields that are affected by quantum confinement. We compared the results from this work with those of $CsPbBr_3$ QDs in the same size range also experiencing strong quantum confinement to examine the similarities and differences between these two QDs.

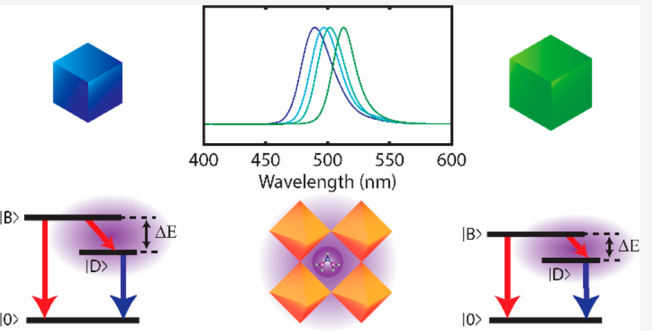

INTRODUCTION

Metal halide perovskite (MHP) semiconductor nanocrystals (NCs) have attracted much attention in photonic and photovoltaic applications[1−9] for their superb photon emitting and charge carrier transporting properties that outperform many existing semiconductor NCs.[10−12] In contrast to traditional semiconductor NCs, where the quantum confinement of excitons has been extensively utilized to tune the bandgap and the energetics of the charge carriers, chemical tuning of the bandgap without resorting to the quantum confinement has been the main approach for MHP nanocrystals.[13−15] Facile exchange of halide ions with continuously variable compositions within the lattice of MHP NCs allowed for continuous tuning of the bandgap and exciton transition energy independently of the quantum confinement. For this reason, many applications of MHP NCs that utilized the emission of photons or transport of charge carriers of varying energy did not require quantum confinement.

On the other hand, the quantum confinement affects not only the energy of the emitted photons and charges derived from the photoexcited exciton in quantum dots (QDs), but also other properties that are sensitive to spatial confinement. The fine structure of the manifold of bright and dark exciton states,[16,17] inter-QD electronic coupling in the QD solids and arrays,[18−20] and intra-QD sensitization by excitons[21−24] are among those affected by the quantum confinement, which also modifies the energy of the emitted photons. With progress in the methods of synthesizing strongly confined MHP QDs,[25,26] the photoluminescence (PL) from dark lowest-energy exciton state was recently observed in strongly confined $CsPbBr_3$ QDs,[27] in contrast to weakly confined $CsPbBr_3$ NCs having the bright lowest-energy exciton state.[28] The inversion of the relative energy levels of the bright and dark states determined by the size-dependent exchange energy of electron and hole was considered to be responsible for the difference between the weakly and strongly confined $CsPbBr_3$ NCs.[17] Auger decay of excitons is another process that is highly dependent on the size of the QDs, with the biexciton lifetime following a universal volume scaling.[29−31]

So far, studies in strongly quantum-confined MHP QDs have been performed more in fully inorganic MHP systems compared to the hybrid MHP systems with organic A-site

Received: August 8, 2022
Revised: October 8, 2022
Published: October 20, 2022

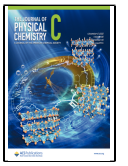

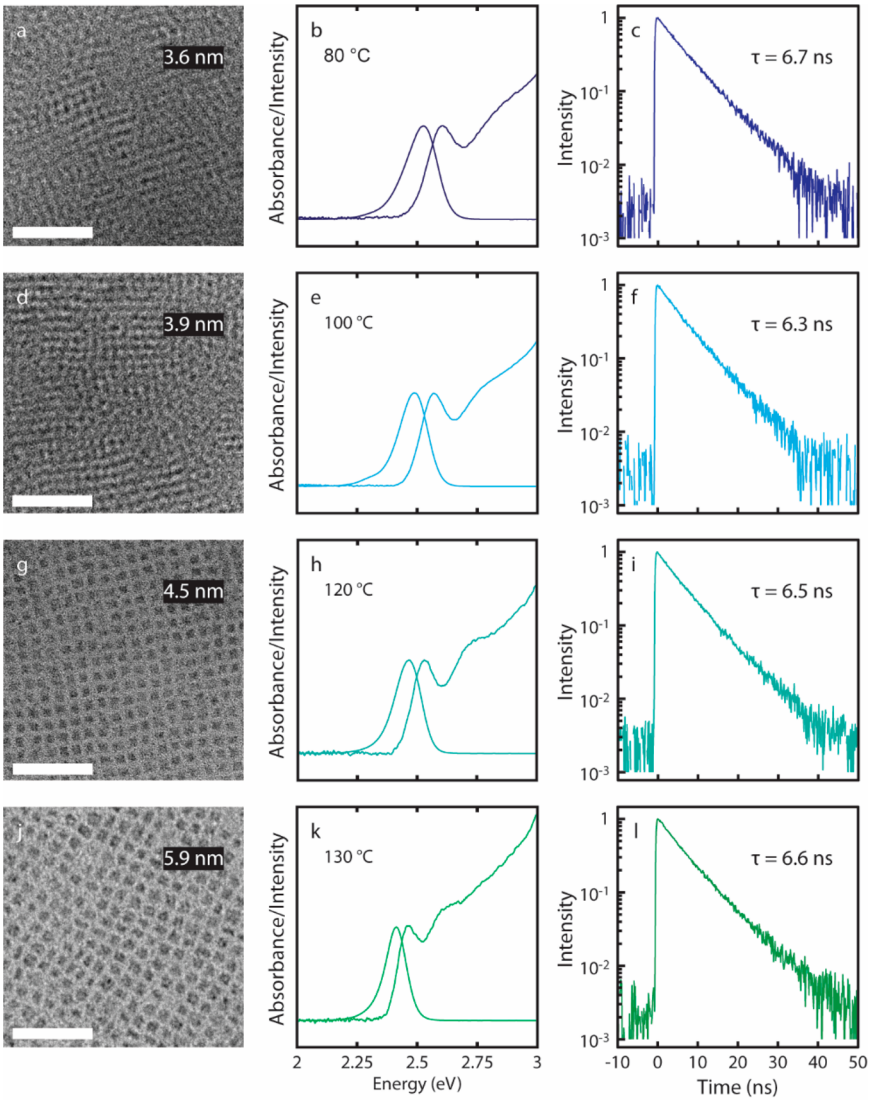

Figure 1. TEM images (left panels), absorption and PL spectra (middle panels) and time-dependent PL intensities (right panels) of $FAPbBr_3$ QDs of different sizes: (a–c) 3.6 nm, (d–f) 3.9 nm, (g–i) 4.5 nm, and (j–l) 5.9 nm. Scale bars in the TEM images are 50 nm.

cations that exhibit several unique features absent in fully inorganic MHP systems. In bulk and nonconfined hybrid MHP, the role of librational motion of the organic cations such as methylammonium (MA^+) or formamidinium (FA^+) ion on the charge carrier screening and its effect on the charge carrier transport have been studied extensively.[32−36] The coupling of exciton transition with the internal nuclear motions of the organic cation is another phenomenon unique to the hybrid MHP systems that is absent in fully inorganic MHP NCs.[37]

In this work, we synthesized strongly quantum-confined $FAPbBr_3$ QDs and investigated their exciton PL spectra and relaxation dynamics at various temperatures and external magnetic fields. In addition to examining the quantum confinement effect on exciton transition energy at ambient temperature, information on exciton fine structure was also obtained from the dynamic exciton PL spectra at 5 K and under an external magnetic field. We also compared the results from $FAPbBr_3$ QDs with those of fully inorganic $CsPbBr_3$ QDs in the similar size range from the earlier studies to examine the similarities and differences between the two strongly quantum-confined MHP QDs.

EXPERIMENTAL METHODS

Synthesis of $FAPbBr_3$ QDs. $FAPbBr_3$ QDs in the size range of 3.6−6.2 nm were synthesized using the procedure modified from the previously reported method for the synthesis of larger $FAPbBr_3$ NCs in weakly confined regime.[38] Modifications were made to the reaction temperature, preparation of the precursor solutions, and product purification to control the size in the strongly confined regime. Briefly, the Br precursor was prepared by dissolving oleylammonium bromide (OLAB, 200 mg) in 2 mL of 1-octadecene (ODE) at 120 °C under N_2 atmosphere after degassing at 120 °C for 30 min on a Schlenk line. FA/Pb precursor was prepared by dissolving lead acetate trihydrate (76 mg) and formamidinium acetate (80 mg) in the mixture of ODE (8 mL) and oleic acid (OA, 2 mL) under N_2 atmosphere after degassing at 120 °C for 30 min. The Br precursor solution was rapidly injected into the FA/Pb precursor solution to initiate the reaction at each given reaction temperature (80−130 °C) that produced the QDs of different size. After 30 s of reaction, the reaction was quenched by rapidly cooling the reactant mixture to 40 °C with an ice−water bath. The reaction product was centrifuged

https://doi.org/10.1021/acs.jpcc.2c05661
J. Phys. Chem. C 2022, 126, 18366−18373

to remove the unreacted salt. The product QDs in the supernatant were recovered by precipitation with methyl acetate and subsequent redispersion in hexane. The average size of the QDs was determined from the transmission electron microscopy (TEM) images obtained with a FEI Tecnai G2 F20 ST FE-TEM instrument at 200 kV.

Spectroscopic Characterization. Steady state absorption and PL spectra of the QDs dispersed in hexane were obtained with an Ocean Optics CCD spectrometer (USB2000 or QE65). The PL quantum yield of the QDs solutions at room temperature was measured using quinine sulfate in 0.05 M sulfuric acid as the reference with known quantum yield of 54%, and evaluated with 350 nm excitation. The PL lifetime of the QD solutions at room temperature was measured using a time-correlated single photon counting setup (PicoHarp 300) equipped with an avalanche photodiode (MPD PDM series) under 50 ps pulsed excitation at 405 nm (PicoQuant, P-C-405). Temperature-dependent steady state PL spectra of the QDs were obtained using an open-cycle optical cryostat (Janis ST-100) under 405 nm cw excitation (RGBLase, FBB-405-200-FM-E-1-0). Time-resolved PL spectra of the QD samples at 5 K were obtained in an open-cycle cryostat (Oxford Instruments Microstat-HE) using a streak camera (Hamamatsu, C14831) coupled to an imaging spectrograph (Princeton Instruments, Acton SpectraPro SP-2300) under 405 nm, 45 ps pulsed excitation (Horiba, 45 ps). Time-dependent PL intensities under the magnetic field were measured in a magneto-optical cryostat (Cryovac) with 0−8 T of magnetic field provided by a superconducting magnet under Faraday geometry. For this measurement, the QD samples were excited with 405 nm, 150 ns pulses and the time-dependent PL intensities were recorded with a time-correlated single photon counting instrument (PicoHarp 300). For all the measurements made in the cryostat, QDs embedded in a polystyrene (PS) matrix were used, which were prepared by drop-casting QDs dispersed in PS/toluene solution (1% PS by weight) on a sapphire window and drying under vacuum.

RESULTS AND DISCUSSION

Figure 1 shows the TEM images, absorption and PL spectra, and time-dependent PL intensities of strongly quantum-confined $FAPbBr_3$ QDs of varying sizes dispersed in hexane at room temperature. Table 1 summarizes the average size of the QDs, the exciton absorption and PL peak, and the PL lifetime for all $FAPbBr_3$ QDs shown in Figure 1. The TEM images show that all the QDs studied here have approximately a cubic morphology with a size distribution of <5% (see Figure S1 in the Supporting Information). The reaction temperature that was varied to control the size is indicted in each panel showing the absorption and PL spectra. Both exciton absorption and PL peaks show a blueshift with decreasing QD size resulting from the quantum confinement, since the size of the QDs are smaller than twice the reported exciton Bohr radius of ∼3.5 nm.[39] The room-temperature PL data show a single-exponential decay with the lifetimes in the range of 6.3−6.7 ns and a PL quantum yield of ∼65% for all $FAPbBr_3$ QDs studied here, exhibiting a relatively weak size dependence. The radiative lifetime estimated from the PL lifetime and PL quantum yield is ∼10 ns for these QDs, which is much shorter than the ∼30 ns radiative lifetime reported in the weakly or nonconfined NCs.[38] The size-dependent bandgap of $FAPbBr_3$ QDs is compared to that of $CsPbBr_3$ QDs in the same size ranges reported in the earlier study[25] in Figure S2 of Supporting Information. The bulk bandgaps of $CsPbBr_3$ and $FAPbBr_3$ QDs are similar, 2.36 and 2.29 eV, respectively, since the band edge levels are mainly composed of the molecular orbitals of Pb nonbonding and Pb−Br antibonding orbitals.[40] The variation of the exciton absorption peak with the size relative to the bulk bandgap shown in Figure S2 is also very similar in both $CsPbBr_3$ and $FAPbBr_3$ QDs. This similarity between $FAPbBr_3$ and $CsPbBr_3$ QDs is expected considering their close exciton Bohr radii of ∼3.5 nm[13,39] and only moderate difference in the dielectric constants ($\varepsilon_r \sim 5$ in $CsPbBr_3$ QDs and $\varepsilon_r \sim 8.6$ in $FAPbBr_3$ QDs).[13,39,41] In large nonconfined size regime, the presence of polaronic confinement of exciton has been suggested in $CsPbBr_3$ NCs although it is unclear whether $FAPbBr_3$ NCs behave similarly to $CsPbBr_3$ NCs.[42]

Figure 2 shows the temperature-dependent steady state PL spectra of $FAPbBr_3$ QDs embedded in polystyrene (PS) matrix in the temperature range of 78−295 K. The temperature-dependent PL peak energy (E_{peak}) and full width at half-maximum (Γ) are also plotted next to the PL spectra. $FAPbBr_3$ QDs of all sizes studied here show a continues and monotonous redshift of E_{peak} with decreasing temperature, which reflects the temperature-dependent bandgap affected by the lattice dilation and electron−phonon coupling.[43] $FAPbB_3$ QDs exhibit the redshift of E_{peak} down to ∼150 K and becomes much less sensitive to the temperature below ∼150 K with no sign of phase transition in the PL spectra previously reported for bulk films.[44] The temperature-shift of E_{peak} in strongly quantum-confined $FAPbB_3$ QDs generally mirrors that of the larger nonconfined $FAPbB_3$ NCs reported previously[44,45] with no particular effect of strong confinement. Compared to $CsPbBr_3$ QDs in the similar size range studied recently,[46] $FAPbBr_3$ QDs exhibit a more monotonous temperature dependence of E_{peak}. In $CsPbBr_3$ QDs, dE_{peak}/dT changed the sign at ∼200 K that was interpreted as the result of different contributions of acoustic and optical phonons to the electron−phonon coupling having the opposite signs of dE_{peak}/dT.[47] Such an inversion of the sign of dE_{peak}/dT is absent in $FAPbBr_3$ QDs. The temperature-dependent Γ of the PL spectra contributed by the inhomogeneous broadening and electron−phonon coupling shows generally larger values for the smaller QDs, which has also been observed in other QDs including $CsPbBr_3$ QDs and II−VI QDs.[46,48] Overall, the size- and temperature-dependent Γ of the PL from $FAPbBr_3$ QDs does not deviate much from typical behavior expected from the colloidal semiconductor QDs.

In previous studies of $CsPbBr_3$ QDs, imposing a strong quantum confinement modified the exciton fine structure, notably pushing the dark exciton level further below the bright exciton level and increasing the dark exciton lifetime (τ_D) with increasing quantum confinement.[27,49] In weakly confined

Table 1. Average QD Size, Absorption, and PL Peak and PL Lifetime at Room Temperature[a]

QD size	E_{abs}	E_{PL}	τ
3.6 nm	2.62 eV	2.53 eV	6.7 ns
3.9 nm	2.58 eV	2.49 eV	6.3 ns
4.5 nm	2.54 eV	2.46 eV	6.6 ns
5.9 nm	2.47 eV	2.41 eV	6.5 ns

[a] E_{abs} and E_{PL} are the energy of the absorption and PL peak, respectively. τ is the single-exponential decay time constant of the PL.

https://doi.org/10.1021/acs.jpcc.2c05661
J. Phys. Chem. C 2022, 126, 18366−18373

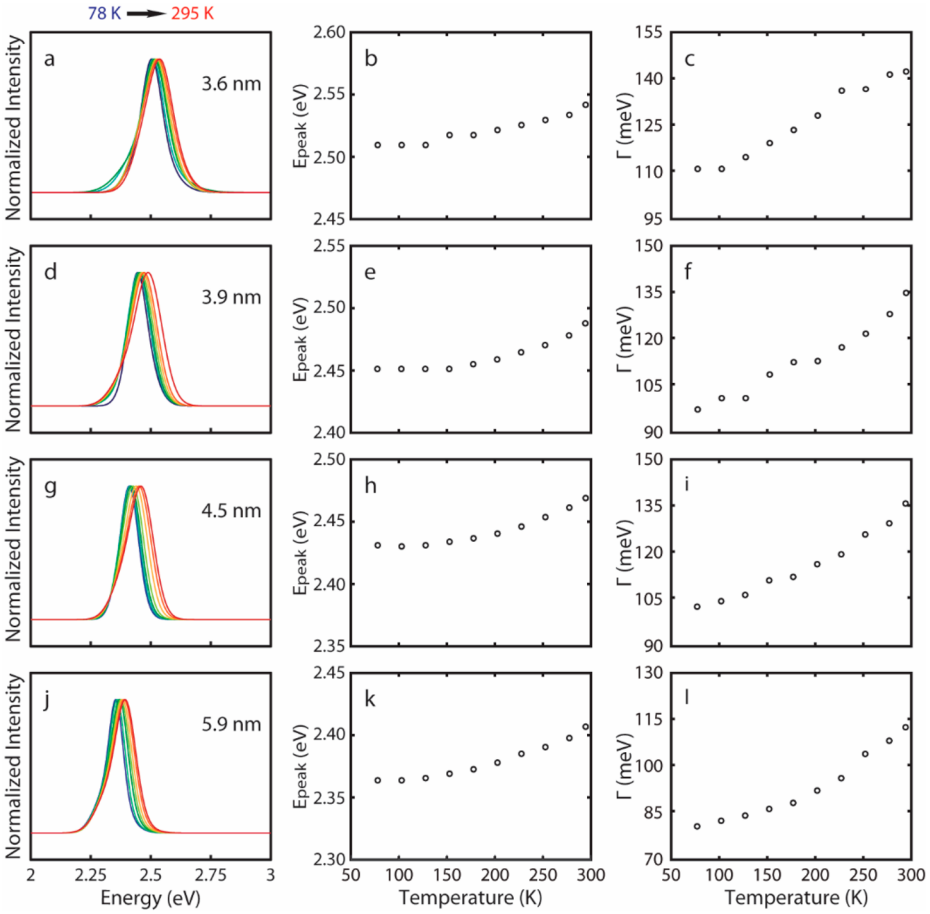

Figure 2. Temperature-dependent PL spectra (left panel), PL peak energy (E_{peak}, middle panel), and full width at half-maximum (Γ, right panel) of $FAPbBr_3$ QDs of different sizes in the temperature range of 78−295 K. The sizes of the QDs are indicated in the panels showing the PL spectra.

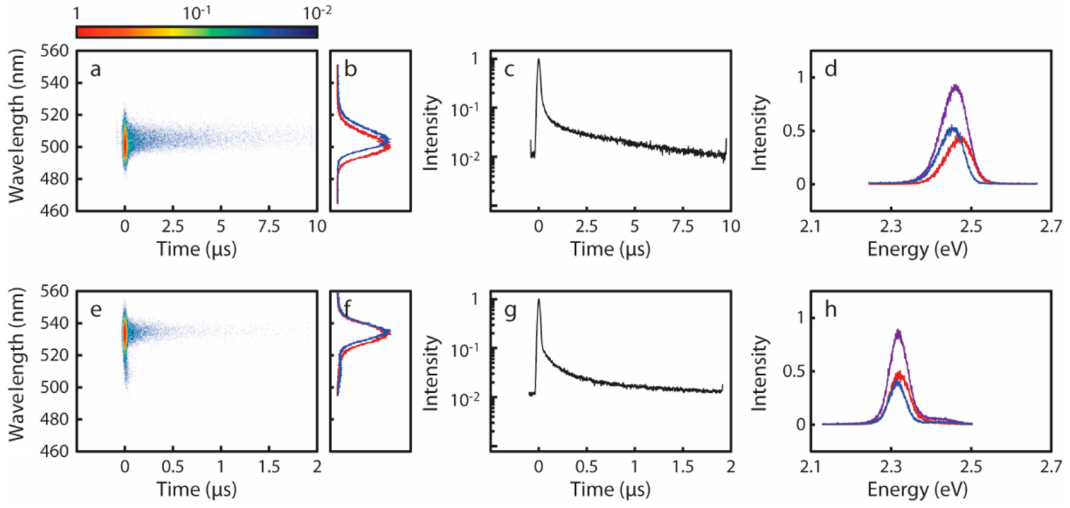

Figure 3. (a, e) Time-resolved PL spectra, (b, f) time gated PL spectra at short (red) and long (blue) time windows, (c, g) time-dependent integrated PL intensity, and (d, h) PL spectra decomposed into bright (red) and dark (blue) exciton PL at 5 K for $FAPbBr_3$ QDs of 2 sizes. (a, b, c, d) 3.6 nm, (e, f, g, h) 6.2 nm.

$FAPbBr_3$ NCs (9.2 nm), a recent study of single-particle PL reported that dark exciton level lies 2.5 meV below bright exciton.[50] To examine whether the quantum confinement has the same effect on the bright-dark level splitting ($\Delta E_{BD} = E_{bright} - E_{dark}$) and τ_D as in $CsPbBr_3$ QDs, we compared the time-dependent PL spectra of $FAPbBr_3$ QDs of different sizes (3.6 and 6.2 nm) at 5 K. At this temperature, dark exciton PL distinguishable from bright exciton PL as the μs-decay component is clearly visible in Figure 3a and e. The time-dependent PL intensities of both QDs are shown in Figure 3c and g, where the slow decay component of the PL (time constant: τ_{slow}) attributed to dark exciton is well-separated

https://doi.org/10.1021/acs.jpcc.2c05661
J. Phys. Chem. C 2022, 126, 18366−18373

Table 2. Spectroscopic Parameters and Lifetimes of Exciton PL at 5 K Shown in Figure 3[a]

QD size	λ_B (E_B)	λ_D (E_D)	ΔE_{BD}	τ_{fast}	τ_{slow} (τ_D)
3.6 nm	500.5 nm (2.4772 eV)	504.3 nm (2.4586 eV)	18.6 meV	0.39 ns	3.1 μs
6.2 nm	533.4 nm (2.3244 eV)	534.8 nm (2.3184 eV)	6.0 meV	0.53 ns	1.2 μs

[a] λ_B (E_B) and λ_D (E_D) are the wavelengths (energy) for bright and dark exciton PL, ΔE_{BD} is the bright-dark level splitting ($E_B - E_D$), and τ_{fast} and τ_{slow} are the time constants for the fast and slow decay components of the PL respectively. τ_{slow} at 5 K is also interpreted as the dark exciton lifetime (τ_D).

from the faster decay component (time constant: τ_{fast}) attributed to bright exciton. Magneto-fluorescence data that further supports the slow decay component of the PL to dark exciton will be discussed further below. τ_{slow} was determined from the fitting of the data in Figure 3c and g. τ_{fast} that is in sub-ns time scale was determined from a separate set of time-dependent PL spectra obtained in several ns time windows providing the sufficient time resolution as shown in Figure S3 in Supporting Information. The sub-ns and μs components of the PL can also be separated spectrally by integrating the time-resolved PL spectra in different time windows. This allows decomposing the PL spectra into the contributions from bright and dark exciton PL as shown in Figure 3b, d, f and h, where the splitting between the two peaks is interpreted as ΔE_{BD}.[27] Table 2 summarizes the peak wavelength for the bright (λ_B) and dark (λ_D) exciton PL, ΔE_{BD}, and the two PL decay time constants (τ_{fast} and τ_{slow}) for the $FAPbBr_3$ QDs of the two different sizes.

It is important to note that ΔE_{BD} in Table 2 is larger for the smaller $FAPbBr_3$ QDs and that ΔE_{BD} values of both QDs are larger than ΔE_{BD} of 2.5 meV reported for 9.2 nm $FAPbBr_3$ NCs in an earlier study.[50] The same trend, i.e., increasing ΔE_{BD} with increasing quantum confinement, was also observed in the strongly confined $CsPbBr_3$ QDs and NPLs.[49,51] This was explained by the increasing electron−hole exchange energy with decreasing QD volume resulting in the increase of ΔE_{BD}. Therefore, one can conclude that both $FAPbBr_3$ QDs and $CsPbBr_3$ QDs exhibit the same effect of confinement-enhanced exchange energy in their size-dependent ΔE_{BD}. In the larger weakly confined NCs, on the other hand, $CsPbBr_3$ and $FAPbBr_3$ are reported to exhibit the opposite bright and dark exciton level order, i.e., negative ΔE_{BD} for $CsPbBr_3$ and positive ΔE_{BD} $FAPbBr_3$. This was considered due to the difference in the balance between the two opposing contributions, i.e., Rashba effect and exchange interaction, in determining the relative ordering of bright and dark exciton level. However, the enhanced electron−hole exchange interaction by the quantum confinement should be the dominating factor for both $CsPbBr_3$ and $FAPbBr_3$ QDs in strongly confined regime, therefore placing the dark state below the bright state with increasing ΔE_{BD} with increasing confinement.[17]

In the exciton level scheme, where the bright state is located above the dark state, we interpret τ_{fast} as the decay time constant for the bright exciton level via the recombination of bright exciton and bright-to-dark transition following the same analysis made for $CsPbBr_3$ QDs in our earlier study.[27] Since 5 K is a sufficiently low temperature to effectively prevent the thermal excitation of the dark state to the bright state, τ_{slow} can be interpreted as the dark exciton lifetime (τ_D). Compared to τ_D of $CsPbBr_3$ QDs of comparable sizes,[27,49] τ_D values of $FAPbBr_3$ QDs are several times smaller (see Table S2 in the Supporting Information), while the smaller τ_D of $FAPbBr_3$ QDs may be interpreted as the stronger bright-dark level mixing if the nonradiative decay of dark state at 5 K is negligible. However, more extensive temperature-dependent PL spectra and PL quantum yield data as well as further theoretical studies will be required to make a more conclusive interpretation of the shorter τ_D.

Since the external magnetic field mixes bright and dark exciton states in MHP NCs, which gives more oscillator strength to the dark excitons and accelerates the relaxation of dark excitons, we examined the effect of an external magnetic field on τ_D of $FAPbBr_3$ QDs of varying sizes. Figure 4 shows

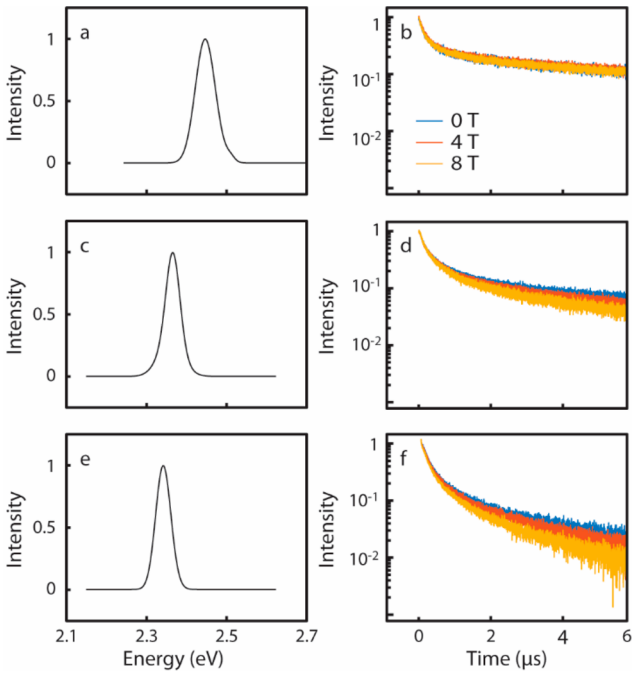

Figure 4. Steady state PL spectra (a, c, e) and magnetic field-dependent PL decay curves (b, d, f) of $FAPbBr_3$ QDs of different sizes measured at 5 K. (a, b) 3.7 nm, (c, d) 5.2 nm ,and (e, f) 5.7 nm.

the time-dependent PL intensities of $FAPbBr_3$ QDs of three different sizes at 5 K at varying external magnetic fields together with the steady state PL spectra at 5 K without external magnetic field. This measurement was performed using a relatively long excitation pulse (405 nm, 150 ns), which does not resolve the fast decay component of bright exciton, therefore only the slow decay component of the PL was examined as a function of external magnetic field. Table 3 summarizes τ_D at 0, 4, and 8 T of magnetic field. With the decreasing size of $FAPbBr_3$ QDs, τ_D becomes less sensitive to the magnetic field, which is consistent with the expectation from the perturbation theory that predicts the stronger mixing of the two states by the perturbation (magnetic field) with the smaller energy gap. It is interesting to see that the smallest $FAPbBr_3$ QDs (3.7 nm) show nearly constant τ_D between 0 and 8 T, whereas $CsPbBr_3$ QDs of similar size showed

https://doi.org/10.1021/acs.jpcc.2c05661
J. Phys. Chem. C 2022, 126, 18366−18373

Table 3. Dark Exciton PL Lifetime of Different Sized $FAPbBr_3$ QDs at Varying External Magnetic Fields at 5 K[a]

QD size	E_{PL}	$\tau_{D,0T}$	$\tau_{D,4T}$	$\tau_{D,8T}$
3.7 nm	2.4498 eV	2.8 μs	2.8 μs	2.8 μs
5.2 nm	2.3684 eV	2.2 μs	2.1 μs	1.9 μs
5.7 nm	2.3451 eV	1.9 μs	1.6 μs	1.2 μs

[a] E_{PL} is the PL peak energy. $\tau_{D,0T}$, $\tau_{D,4T}$, and $\tau_{D,8T}$ are the dark exciton PL lifetime at 0, 4 and 8 T respectively.

significantly stronger dependence of τ_D on the magnetic field in the earlier study.[27] The difference in the sensitivity of τ_D to the magnetic field between $CsPbBr_3$ QDs and $FAPbBr_3$ QDs is not clear yet. Whether the asymmetry and the presence of internal nuclear degrees of freedom of the organic cation play a role in this difference will be an interesting question to answer in future studies.

CONCLUSION

We synthesized strongly quantum-confined $FAPbBr_3$ QDs and investigated the effect of quantum confinement on the exciton PL properties and exciton fine structure. The strongly quantum-confined $FAPbBr_3$ QDs show an increasing bandgap with decreasing QD size, which is comparable in the magnitude to that of $CsPbBr_3$ QDs in a similar size range. The PL of $FAPbBr_3$ QDs shows a redshift and line width narrowing with decreasing temperature in the 78−295 K range, which is also qualitatively similar to the behavior of $CsPbBr_3$ QDs. Time-resolved PL spectra of $FAPbBr_3$ QDs at 5 K revealed intense PL from the dark lowest-energy exciton state with μs lifetime. The bright-dark level splitting (ΔE_{BD}) increased with increasing quantum confinement, consistent with the expectation from the confinement-enhanced electron−hole exchange energy that increases ΔE_{BD}, which is also in line with the observation made in $CsPbBr_3$ QDs. On the other hand, the dark exciton lifetime (τ_D) was significantly shorter than that of the comparably sized $CsPbBr_3$ QDs, possibly suggesting the stronger mixing of bright and dark states. Under the external magnetic field, τ_D decreased at the higher field with decreasing sensitivity of τ_D to the magnetic field with decreasing QD size. When compared to $CsPbBr_3$ QDs of the same size, the shortening of τ_D via magnetic mixing is less in $FAPbBr_3$ QDs, although whether the organic cation plays a role in this difference is uncertain.

ASSOCIATED CONTENT

Supporting Information

The Supporting Information is available free of charge at https://pubs.acs.org/doi/10.1021/acs.jpcc.2c05661.

Size distribution of QDs, size-dependent exciton absorption of $CsPbBr_3$ QDs and $FAPbBr_3$ QDs, additional time-resolved PL spectra of $FAPbBr_3$ QDs at 5 K in 5 ns time window (PDF)

AUTHOR INFORMATION

Corresponding Author

Dong Hee Son − *Department of Chemistry, Texas A&M University, College Station, Texas 77843, United State;* orcid.org/0000-0001-9002-5188; Email: dhson@tamu.edu

Authors

Xueting Tang − *Department of Chemistry, Texas A&M University, College Station, Texas 77843, United State*

Mohit Khurana − *Department of Physics and Astronomy, Texas A&M University, College Station, Texas 77843, United State*

Daniel Rossi − *Department of Chemistry, University of Michigan, Ann Arbor, Michigan 48109, United State*

Lanyin Luo − *Department of Physics and Astronomy, Texas A&M University, College Station, Texas 77843, United State*

Alexey V. Akimov − *Department of Physics and Astronomy, Texas A&M University, College Station, Texas 77843, United State*

Complete contact information is available at: https://pubs.acs.org/10.1021/acs.jpcc.2c05661

Notes

The authors declare no competing financial interest.

ACKNOWLEDGMENTS

This research was supported by National Science Foundation (CHE-2003961).

REFERENCES

(1) Tan, Z. K.; Moghaddam, R. S.; Lai, M. L.; Docampo, P.; Higler, R.; Deschler, F.; Price, M.; Sadhanala, A.; Pazos, L. M.; Credgington, D.; et al. Bright light-emitting diodes based on organometal halide perovskite. *Nat. Nanotechnol.* **2014**, *9*, 687−692.

(2) Chiba, T.; Hayashi, Y.; Ebe, H.; Hoshi, K.; Sato, J.; Sato, S.; Pu, Y. J.; Ohisa, S.; Kido, J. Anion-exchange red perovskite quantum dots with ammonium iodine salts for highly efficient light-emitting devices. *Nat. Photonics* **2018**, *12*, 681−687.

(3) Lin, K.; Xing, J.; Quan, L. N.; de Arquer, F. P. G.; Gong, X.; Lu, J.; Xie, L.; Zhao, W.; Zhang, D.; Yan, C.; et al. Perovskite light-emitting diodes with external quantum efficiency exceeding 20%. *Nature* **2018**, *562*, 245−248.

(4) Quan, L. N.; Rand, B. P.; Friend, R. H.; Mhaisalkar, S. G.; Lee, T. W.; Sargent, E. H. Perovskites for Next-Generation Optical Sources. *Chem. Rev.* **2019**, *119*, 7444−7477.

(5) Kojima, A.; Teshima, K.; Shirai, Y.; Miyasaka, T. Organometal halide perovskites as visible-light sensitizers for photovoltaic cells. *J. Am. Chem. Soc.* **2009**, *131*, 6050−6051.

(6) Lee, M. M.; Teuscher, J.; Miyasaka, T.; Murakami, T. N.; Snaith, H. J. Efficient hybrid solar cells based on meso-superstructured organometal halide perovskites. *Science* **2012**, *338*, 643−647.

(7) Kim, H. S.; Lee, C. R.; Im, J. H.; Lee, K. B.; Moehl, T.; Marchioro, A.; Moon, S. J.; Humphry-Baker, R.; Yum, J. H.; Moser, J. E.; et al. Lead iodide perovskite sensitized all-solid-state submicron thin film mesoscopic solar cell with efficiency exceeding 9%. *Sci. Rep.* **2012**, *2*, 591.

(8) Burschka, J.; Pellet, N.; Moon, S. J.; Humphry-Baker, R.; Gao, P.; Nazeeruddin, M. K.; Gratzel, M. Sequential deposition as a route to high-performance perovskite-sensitized solar cells. *Nature* **2013**, *499*, 316−319.

(9) Jena, A. K.; Kulkarni, A.; Miyasaka, T. Halide Perovskite Photovoltaics: Background, Status, and Future Prospects. *Chem. Rev.* **2019**, *119*, 3036−3103.

(10) Stranks, S. D.; Eperon, G. E.; Grancini, G.; Menelaou, C.; Alcocer, M. J.; Leijtens, T.; Herz, L. M.; Petrozza, A.; Snaith, H. J. Electron-hole diffusion lengths exceeding 1 micrometer in an organometal trihalide perovskite absorber. *Science* **2013**, *342*, 341−344.

(11) Yin, W. J.; Shi, T. T.; Yan, Y. F. Unusual defect physics in $CH_3NH_3PbI_3$ perovskite solar cell absorber. *Appl. Phys. Lett.* **2014**, *104*, 063903.

(12) Kang, J.; Wang, L. W. High Defect Tolerance in Lead Halide Perovskite $CsPbBr_3$. *J. Phys. Chem. Lett.* **2017**, *8*, 489−493.
(13) Protesescu, L.; Yakunin, S.; Bodnarchuk, M. I.; Krieg, F.; Caputo, R.; Hendon, C. H.; Yang, R. X.; Walsh, A.; Kovalenko, M. V. Nanocrystals of Cesium Lead Halide Perovskites ($CsPbX_3$, X = Cl, Br, and I): Novel Optoelectronic Materials Showing Bright Emission with Wide Color Gamut. *Nano Lett.* **2015**, *15*, 3692−3696.
(14) Nedelcu, G.; Protesescu, L.; Yakunin, S.; Bodnarchuk, M. I.; Grotevent, M. J.; Kovalenko, M. V. Fast Anion-Exchange in Highly Luminescent Nanocrystals of Cesium Lead Halide Perovskites ($CsPbX_3$, X = Cl, Br, I). *Nano Lett.* **2015**, *15*, 5635−5640.
(15) Parobek, D.; Dong, Y.; Qiao, T.; Rossi, D.; Son, D. H. Photoinduced Anion Exchange in Cesium Lead Halide Perovskite Nanocrystals. *J. Am. Chem. Soc.* **2017**, *139*, 4358−4361.
(16) Leung, K.; Pokrant, S.; Whaley, K. B. Exciton fine structure in CdSe nanoclusters. *Phys. Rev. B* **1998**, *57*, 12291−12301.
(17) Sercel, P. C.; Lyons, J. L.; Wickramaratne, D.; Vaxenburg, R.; Bernstein, N.; Efros, A. L. Exciton Fine Structure in Perovskite Nanocrystals. *Nano Lett.* **2019**, *19*, 4068−4077.
(18) Artemyev, M. V.; Bibik, A. I.; Gurinovich, L. I.; Gaponenko, S. V.; Woggon, U. Evolution from individual to collective electron states in a dense quantum dot ensemble. *Phys. Rev. B* **1999**, *60*, 1504−1506.
(19) Koole, R.; Liljeroth, P.; de Mello Donega, C.; Vanmaekelbergh, D.; Meijerink, A. Electronic coupling and exciton energy transfer in CdTe quantum-dot molecules. *J. Am. Chem. Soc.* **2006**, *128*, 10436−10441.
(20) Tang, X.; Rossi, D.; Cheon, J.; Son, D. H. Effects of Electronic Coupling on Bright and Dark Excitons in a 2D Array of Strongly Confined $CsPbBr_3$ Quantum Dots. *Chem. Mater.* **2022**, *34*, 7181−7189.
(21) Bol, A. A.; Meijerink, A. Long-lived Mn^{2+} emission in nanocrystalline ZnS:Mn^{2+}. *Phys. Rev. B* **1998**, *58*, R15997−R16000.
(22) Beaulac, R.; Archer, P. I.; Ochsenbein, S. T.; Gamelin, D. R. Mn^{2+}-Doped CdSe Quantum Dots: New Inorganic Materials for Spin-Electronics and Spin-Photonics. *Adv. Funct. Mater.* **2008**, *18*, 3873−3891.
(23) Chen, H. Y.; Chen, T. Y.; Berdugo, E.; Park, Y.; Lovering, K.; Son, D. H. Hot Electrons from Consecutive Exciton-Mn Energy Transfer in Mn-Doped Semiconductor Nanocrystals. *J. Phys. Chem. C* **2011**, *115*, 11407−11412.
(24) Parobek, D.; Roman, B. J.; Dong, Y.; Jin, H.; Lee, E.; Sheldon, M.; Son, D. H. Exciton-to-Dopant Energy Transfer in Mn-Doped Cesium Lead Halide Perovskite Nanocrystals. *Nano Lett.* **2016**, *16*, 7376−7380.
(25) Dong, Y.; Qiao, T.; Kim, D.; Parobek, D.; Rossi, D.; Son, D. H. Precise Control of Quantum Confinement in Cesium Lead Halide Perovskite Quantum Dots via Thermodynamic Equilibrium. *Nano Lett.* **2018**, *18*, 3716−3722.
(26) Dong, Y.; Qiao, T.; Kim, D.; Rossi, D.; Ahn, S. J.; Son, D. H. Controlling Anisotropy of Quantum-Confined $CsPbBr_3$ Nanocrystals by Combined Use of Equilibrium and Kinetic Anisotropy. *Chem. Mater.* **2019**, *31*, 5655−5662.
(27) Rossi, D.; Liu, X.; Lee, Y.; Khurana, M.; Puthenpurayil, J.; Kim, K.; Akimov, A. V.; Cheon, J.; Son, D. H. Intense Dark Exciton Emission from Strongly Quantum-Confined $CsPbBr_3$ Nanocrystals. *Nano Lett.* **2020**, *20*, 7321−7326.
(28) Becker, M. A.; Vaxenburg, R.; Nedelcu, G.; Sercel, P. C.; Shabaev, A.; Mehl, M. J.; Michopoulos, J. G.; Lambrakos, S. G.; Bernstein, N.; Lyons, J. L.; et al. Bright triplet excitons in caesium lead halide perovskites. *Nature* **2018**, *553*, 189−193.
(29) Makarov, N. S.; Guo, S.; Isaienko, O.; Liu, W.; Robel, I.; Klimov, V. I. Spectral and Dynamical Properties of Single Excitons, Biexcitons, and Trions in Cesium-Lead-Halide Perovskite Quantum Dots. *Nano Lett.* **2016**, *16*, 2349−2362.
(30) Li, Y.; Ding, T.; Luo, X.; Tian, Y.; Lu, X.; Wu, K. Synthesis and Spectroscopy of Monodispersed, Quantum-Confined $FAPbBr_3$ Perovskite Nanocrystals. *Chem. Mater.* **2020**, *32*, 549−556.
(31) Li, Y.; Luo, X.; Ding, T.; Lu, X.; Wu, K. Size- and Halide-Dependent Auger Recombination in Lead Halide Perovskite Nanocrystals. *Angew. Chem., Int. Ed.* **2020**, *59*, 14292−14295.
(32) Neukirch, A. J.; Nie, W.; Blancon, J. C.; Appavoo, K.; Tsai, H.; Sfeir, M. Y.; Katan, C.; Pedesseau, L.; Even, J.; Crochet, J. J.; et al. Polaron Stabilization by Cooperative Lattice Distortion and Cation Rotations in Hybrid Perovskite Materials. *Nano Lett.* **2016**, *16*, 3809−3816.
(33) Bonn, M.; Miyata, K.; Hendry, E.; Zhu, X. Y. Role of Dielectric Drag in Polaron Mobility in Lead Halide Perovskites. *ACS Energy Lett.* **2017**, *2*, 2555−2562.
(34) Zhu, H.; Miyata, K.; Fu, Y.; Wang, J.; Joshi, P. P.; Niesner, D.; Williams, K. W.; Jin, S.; Zhu, X. Y. Screening in crystalline liquids protects energetic carriers in hybrid perovskites. *Science* **2016**, *353*, 1409−1413.
(35) Frost, J. M.; Walsh, A. What Is Moving in Hybrid Halide Perovskite Solar Cells? *Acc. Chem. Res.* **2016**, *49*, 528−535.
(36) Zhu, X. Y.; Podzorov, V. Charge Carriers in Hybrid Organic-Inorganic Lead Halide Perovskites Might Be Protected as Large Polarons. *J. Phys. Chem. Lett.* **2015**, *6*, 4758−4761.
(37) Pfingsten, O.; Klein, J.; Protesescu, L.; Bodnarchuk, M. I.; Kovalenko, M. V.; Bacher, G. Phonon Interaction and Phase Transition in Single Formamidinium Lead Bromide Quantum Dots. *Nano Lett.* **2018**, *18*, 4440−4446.
(38) Protesescu, L.; Yakunin, S.; Bodnarchuk, M. I.; Bertolotti, F.; Masciocchi, N.; Guagliardi, A.; Kovalenko, M. V. Monodisperse Formamidinium Lead Bromide Nanocrystals with Bright and Stable Green Photoluminescence. *J. Am. Chem. Soc.* **2016**, *138*, 14202−14205.
(39) Levchuk, I.; Osvet, A.; Tang, X.; Brandl, M.; Perea, J. D.; Hoegl, F.; Matt, G. J.; Hock, R.; Batentschuk, M.; Brabec, C. J. Brightly Luminescent and Color-Tunable Formamidinium Lead Halide Perovskite $FAPbX_3$ (X = Cl, Br, I) Colloidal Nanocrystals. *Nano Lett.* **2017**, *17*, 2765−2770.
(40) Brivio, F.; Walker, A. B.; Walsh, A. Structural and electronic properties of hybrid perovskites for high-efficiency thin-film photovoltaics from first-principles. *APL Materials* **2013**, *1*, 042111.
(41) Galkowski, K.; Mitioglu, A.; Miyata, A.; Plochocka, P.; Portugall, O.; Eperon, G. E.; Wang, J. T.-W.; Stergiopoulos, T.; Stranks, S. D.; Snaith, H. J.; et al. Determination of the exciton binding energy and effective masses for methylammonium and formamidinium lead tri-halide perovskite semiconductors. *Energy Environ. Sci.* **2016**, *9*, 962−970.
(42) Baker, H.; Strandell, D.; Kambhampati, P. Emitting State of Bulk $CsPbBr_3$ Perovskite Nanocrystals Reveals a Quantum-Confined Excitonic Structure. *J. Phys. Chem. C* **2020**, *124*, 18816−18822.
(43) Manser, J. S.; Christians, J. A.; Kamat, P. V. Intriguing Optoelectronic Properties of Metal Halide Perovskites. *Chem. Rev.* **2016**, *116*, 12956−13008.
(44) Wright, A. D.; Verdi, C.; Milot, R. L.; Eperon, G. E.; Perez-Osorio, M. A.; Snaith, H. J.; Giustino, F.; Johnston, M. B.; Herz, L. M. Electron-phonon coupling in hybrid lead halide perovskites. *Nat. Commun.* **2016**, *7*, 11755.
(45) Ghosh, S.; Shi, Q.; Pradhan, B.; Kumar, P.; Wang, Z.; Acharya, S.; Pal, S. K.; Pullerits, T.; Karki, K. J. Phonon Coupling with Excitons and Free Carriers in Formamidinium Lead Bromide Perovskite Nanocrystals. *J. Phys. Chem. Lett.* **2018**, *9*, 4245−4250.
(46) Cheng, O. H.; Qiao, T.; Sheldon, M.; Son, D. H. Size- and temperature-dependent photoluminescence spectra of strongly confined $CsPbBr_3$ quantum dots. *Nanoscale* **2020**, *12*, 13113−13118.
(47) Saran, R.; Heuer-Jungemann, A.; Kanaras, A. G.; Curry, R. J. Giant Bandgap Renormalization and Exciton-Phonon Scattering in Perovskite Nanocrystals. *Adv. Opt. Mater.* **2017**, *5*, 1700231.
(48) Jing, P. T.; Zheng, J. J.; Ikezawa, M.; Liu, X. Y.; Lv, S. Z.; Kong, X. G.; Zhao, J. L.; Masumoto, Y. Temperature-Dependent Photoluminescence of CdSe-Core CdS/CdZnS/ZnS-Multishell Quantum Dots. *J. Phys. Chem. C* **2009**, *113*, 13545−13550.
(49) Rossi, D.; Qiao, T.; Liu, X.; Khurana, M.; Akimov, A. V.; Cheon, J.; Son, D. H. Size-dependent dark exciton properties in

https://doi.org/10.1021/acs.jpcc.2c05661
J. Phys. Chem. C 2022, 126, 18366−18373

cesium lead halide perovskite quantum dots. *J. Chem. Phys.* **2020**, *153*, 184703.
(50) Tamarat, P.; Bodnarchuk, M. I.; Trebbia, J. B.; Erni, R.; Kovalenko, M. V.; Even, J.; Lounis, B. The ground exciton state of formamidinium lead bromide perovskite nanocrystals is a singlet dark state. *Nat. Mater.* **2019**, *18*, 717−724.
(51) Gramlich, M.; Swift, M. W.; Lampe, C.; Lyons, J. L.; Doblinger, M.; Efros, A. L.; Sercel, P. C.; Urban, A. S. Dark and Bright Excitons in Halide Perovskite Nanoplatelets. *Adv. Sci.* **2022**, *9*, No. e2103013.

https://doi.org/10.1021/acs.jpcc.2c05661
J. Phys. Chem. C 2022, 126, 18366−18373